FLUCOME 2009
10th International Conference on Fluid Control, Measurements, and Visualization
August 17–21, 2009, Moscow, Russia

PREDICTION OF THE POLLEN SCATTERING AND INVASIVE BEHAVIOR

Ichiro Nakane[1] and Takeshi Ide[2]

ABSTRACT

Japanese cedar pollinosis is a very serious problem, because the prevalence is considered more than 20% in Japanese. This pollen is carried by the wind, and it invades our nose holes by taking in breath. This paper describes to predict the pollen scattering behavior in the wind and the pollen invasive behavior in taking in breath.

The pollen scattering behavior is studied by the numerical calculation and the wind tunnel experiment. The velocity profiles of numerical calculation agree very well with the experimentally measured one by using the optical measurement techniques. The mean flow behavior of the pollen can be predicted by the calculation method of this study.

The pollen invasive behavior into the nose hole is studied by using the phantom model. The velocity profiles around the nose hole of the phantom model were numerically calculated and optically measured too. The influence of air velocity of suction breath on the pollen invasion is cleared.

Keywords: Pollen Transport, Multi-phase Flow, Numerical Simulation, Optical Measurement

INTRODUCTION

Japanese cedar (Cryptomeria japonica) pollinosis is the most common allergic diseases in Japan, with more than 20% of the population being affected, and an economic loss caused by this pollinosis is estimated about $10 billion or more.

The pollen of Japanese cedar is carried by the wind, but the aerodynamic diameter d_a of this pollen is comparatively large. We estimate the mean d_a of Japanese cedar pollen at 35μm in this study. Consequently, the pollen flow behavior must be different from the wind behavior. The pollen falls when the wind is weak, and it is blown up by the strong wind. If the pollen flow behavior is completely corresponding to the wind behavior, the range of Japanese cedar growth will be very broad and the peculiar distribution of Japanese cedar must be confused. This difference between the airflow and the pollen flow behavior must influence the concentration of the pollen in suction air of breath. We guess that the pollen concentration in suction air increases as we take in breath powerfully and deeply.

[1] Corresponding author: Dep. of Mech. Eng., Fac. of Eng. , Kanagawa Inst. of Tech., e-mail: inakane@me.kanagawa-it.ac.jp
[2] Dep. of Chem., School of Med., Nara Med. Univ.

This study aims to clarify the behavior of the pollen scattering and invading our nose holes and to confirm the validity of the prediction method. We did the followings in this study, and the results of the followings are shown and discussed in this paper.

(1) We measured the terminal velocity of the Japanese cedar pollen by the free fall experiment and selected the test particle that has approximately the same aerodynamic diameter of the pollen.

(2) We measured the test particle velocity in the wind by the particle tracking velocimetry. The difference between the air and the test particle velocities is cleared in this paper.

(3) We numerically calculated the air and the test particle velocities in the same condition of the above (2). The prediction method of the pollen scattering behavior is discussed in this paper.

(4) We measured and calculated the particle invasive behavior. The influence of air velocity of suction breath on the pollen invasion is cleared in this paper.

FREE FALL EXPERIMENT TO MEASURE THE TERMINAL VELOCITY OF THE POLLEN

The terminal velocity V_t of the Japanese cedar pollen is measured by the free fall experiment in the pollen exposure chamber. The schema of this chamber is shown as Fig.1. We tried to generate the convection and to put the dust in this chamber as least as possible.

While the Japanese cedar pollens fall in this chamber, they are irradiated with the green laser light sheet and this free falling behavior is recorded by the high-speed video camera. The terminal velocity of them is measured using Particle Tracking Velocimetry (PTV) from these recorded particle images. We obtained the terminal velocity of thirteen hundred particles in total. These measurement results are shown in Fig.2. In this histogram (Fig.2), the vertical axis represents the total number of particles measured by PTV, and the horizontal axis represents the terminal velocity (range of ±1.5mm/s).

Fig. 2 shows that the mean terminal velocity V_{tm} is 38mm/s. We calculated the particle diameter d from this terminal velocity and Stokes' Law for drag. Additionally, we used the already reported particle density. The study of the aerodynamic properties (including the density) of Japanese cedar pollen is very few, but Tang *et al.* (2007) measured its particle diameter and density. Their results are shown as follows.

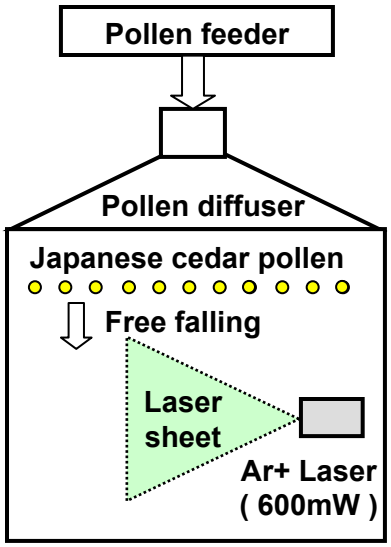

Fig.1 Schema of the pollen exposure chamber

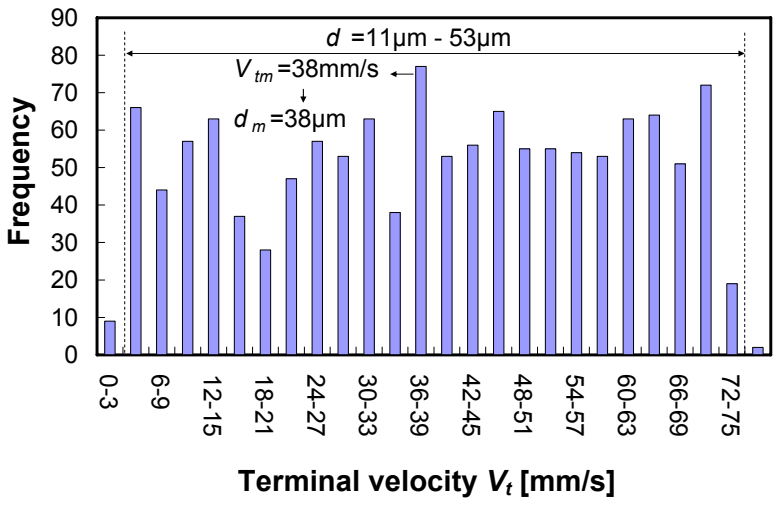

Fig.2 Histogram of the pollen terminal velocity measured by PTV in the chamber (ref. Fig.1)

(1) The diameter of Japanese cedar pollen is in the range from 15μm to 50μm, and its mean is 26.6μm.
(2) The particle density of Japanese cedar pollen is 0.86g/cm^3 and its true density is 1.40g/cm^3.
(3) The terminal velocity that estimates by the above particle diameter and density is 1.9cm/s.

By using the above particle density ρ_p=0.86g/cm^3, the particle diameter d is calculated from the terminal velocity V_t. Fig.2 shows this diameter d is in the range from 11μm to 53μm and its mean d_m is 38μm. This calculated mean diameter d_m is somewhat larger than the above result (1), but Ohashi and Ooka (2001) also show the slightly larger mean diameter 31.1μm by the laser scanning microscope measurement. We consider that this difference of the mean diameter originates in the individual specificity of Japanese cedar and this mean diameter d_m=38μm is adequate.

TEST PARTICLE SUBSTITUTED FOR JAPANESE CEDAR POLLEN

From the above free fall experiment, the mean particle diameter of Japanese cedar pollen is about 38μm. Consequently, the aerodynamic diameter of this pollen is calculated as about 35μm. We selected the test particle that has approximately the same aerodynamic diameter d_a of Japanese cedar pollen, to substitute the test particle for the pollen, because the pollen causes the allergic serious damage to our nose and eyes.

After all, we use Lycopodium clavatum spores as the test particle, because their aerodynamic diameters d_a=33μm are nearly the same as Japanese cedar pollen d_a=35μm and they cause almost no damage to us. The characteristics of them are shown as Table 1 and the picture of them taken by the laser scanning microscope is shown as Fig.3. (*: Copyright permission from The Association of Powder Process Industry and Engineering, JAPAN)

Table 1 The characteristics of the test particle (Test particle : Lycopodium clavatum spores)

Diameter d	from 20μm to 50μm
Mean Diameter d_m	32 [μm]
Terminal velocity by Stokes' Law V_t	32.5 [mm/s]
Aerodynamic Diameter d_a	33 [μm]
Particle Density ρ_p	1.05 [g/cm^3]

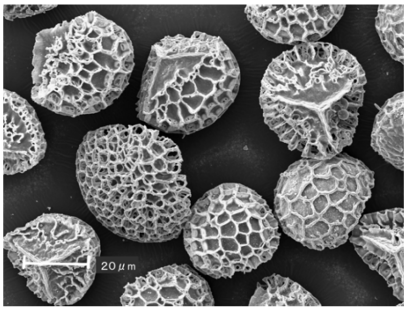

Fig.3 Test particle*

AIR AND PARTICLE FLOW VELOCITIES IN THE FLAT PLATE BOUNDARY LAYER

We used the recirculating wind tunnel and measured the test particle velocities u_{pm} and v_{pm} in the wind, to clarify the difference of flow behavior between the air and the pollen (the test particle). The schema of this experimental apparatus is shown in Fig.4. Fig.4 shows that the flat plate is set up in the recirculating wind tunnel and the test particle is diffused in it with zero initial velocity. The air and the particle velocities profiles in the flat plate boundary layer are measured.

The test particle flows on the flat plate is irradiated with the green laser light sheet, and this flow behavior is recorded by the digital hi-vision video camera. The velocities of the test particle u_{pm} and v_{pm} are calculated by the length of their path lines and the shutter speed of the video camera. Moreover, the x-directional airflow velocity u_m is measured by an air velocity meter.

In the same condition of the above experiment, we numerically calculated the air and the test particle flow velocities in the boundary layer on the flat plate. All governing equations are two-dimensional steady state and are as follows.

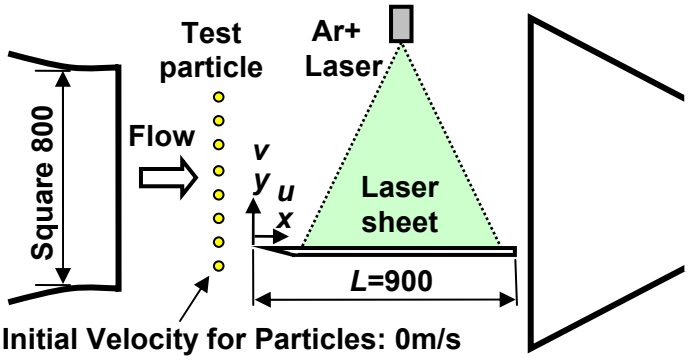

Fig.4 Schema of the experimental apparatus to measure the flat plate boundary layer flow

For the airflow:

(1) Continuity equation

$$\frac{\partial}{\partial y}\left(\frac{\partial u}{\partial x}+\frac{\partial v}{\partial y}\right)=0$$

(2) Navier-Stokes equation

$$\rho\left(u\frac{\partial u}{\partial x}+v\frac{\partial u}{\partial y}\right)=\frac{\partial}{\partial x}\left\{(\mu+\mu_t)\frac{\partial u}{\partial x}\right\}+\frac{\partial}{\partial y}\left\{(\mu+\mu_t)\frac{\partial u}{\partial y}\right\}$$

$$\mu_t=\rho\, C_\mu f_\mu \frac{k^2}{\varepsilon} \qquad C_\mu=0.09,\quad f_\mu=\exp\left(\frac{-2.5}{1+R_t/50}\right),\quad R_t=\frac{\rho k^2}{\mu\varepsilon}$$

(3) Jones & Launder low-Re k-ε model

$$\rho\left(u\frac{\partial k}{\partial x}+v\frac{\partial k}{\partial y}\right)=\frac{\partial}{\partial x}\left\{(\mu+\frac{\mu_t}{\sigma_k})\frac{\partial k}{\partial x}\right\}+\frac{\partial}{\partial y}\left\{(\mu+\frac{\mu_t}{\sigma_k})\frac{\partial k}{\partial y}\right\}+G-\rho\varepsilon-2\mu\left(\frac{\partial\sqrt{k}}{\partial y}\right)^2$$

$$\rho\left(u\frac{\partial \varepsilon}{\partial x}+v\frac{\partial \varepsilon}{\partial y}\right)=\frac{\partial}{\partial x}\left\{(\mu+\frac{\mu_t}{\sigma_\varepsilon})\frac{\partial \varepsilon}{\partial x}\right\}+\frac{\partial}{\partial y}\left\{(\mu+\frac{\mu_t}{\sigma_\varepsilon})\frac{\partial \varepsilon}{\partial y}\right\}+C_1 G\frac{\varepsilon}{k}-C_2 f_2\frac{\rho\varepsilon^2}{k}+2\frac{\mu\mu_t}{\rho}\left(\frac{\partial^2 u}{\partial y^2}\right)^2$$

$$G=\mu_t\left\{2\left(\frac{\partial u}{\partial x}\right)^2+2\left(\frac{\partial v}{\partial y}\right)^2+\left(\frac{\partial u}{\partial y}+\frac{\partial v}{\partial x}\right)^2\right\}$$

$$\sigma_k=1.0,\quad \sigma_\varepsilon=1.3,\quad C_1=1.55,\quad C_2=2.0,\quad f_2=1-0.3\exp\left(-R_t^2\right)$$

For the particle:

(4) *x*-Momentum equation

$$u_p\frac{\partial u_p}{\partial x}+v_p\frac{\partial u_p}{\partial y}=\frac{18\mu(u-u_p)}{\rho_p d_m^2}$$

(5) *y*-Momentum equation

$$u_p\frac{\partial v_p}{\partial x}+v_p\frac{\partial v_p}{\partial y}=-\left(1-\frac{\rho}{\rho_p}\right)\mathrm{g}+\frac{18\mu(v-v_p)}{\rho_p d_m^2}$$

The boundary conditions for each velocity are as follows.

(1) The inlet boundary : Measured velocity profiles
(2) The outlet boundary : Fully developed flow
(3) The lower wall boundary : No slip condition
(4) The upper boundary : Mainstream and fully developed flow

The above equations are discretized by finite difference method and solved using the tridiagonal

matrix algorithm (TDMA) with these boundary conditions. The non-dimensional grid size of Δx^* is 10^{-2} and the non-dimensional grid sizes of Δy^* are from 10^{-7} to 10^{-4}. The convergence of each velocity is confirmed by the relative error rate less than 10^{-5}.

These measured and calculated velocities are shown in Fig.5 and 6 for comparison purposes. Fig.5 is the case of mainstream velocity U=3m/s and Fig.6 is U=1.5m/s. In addition, the calculated x-directional velocities of the test particle u_p and the air u are approximately same, and the dotted line for u virtually lies on top of the solid line for u_p in each figure. We can hardly distinguish one from the other.

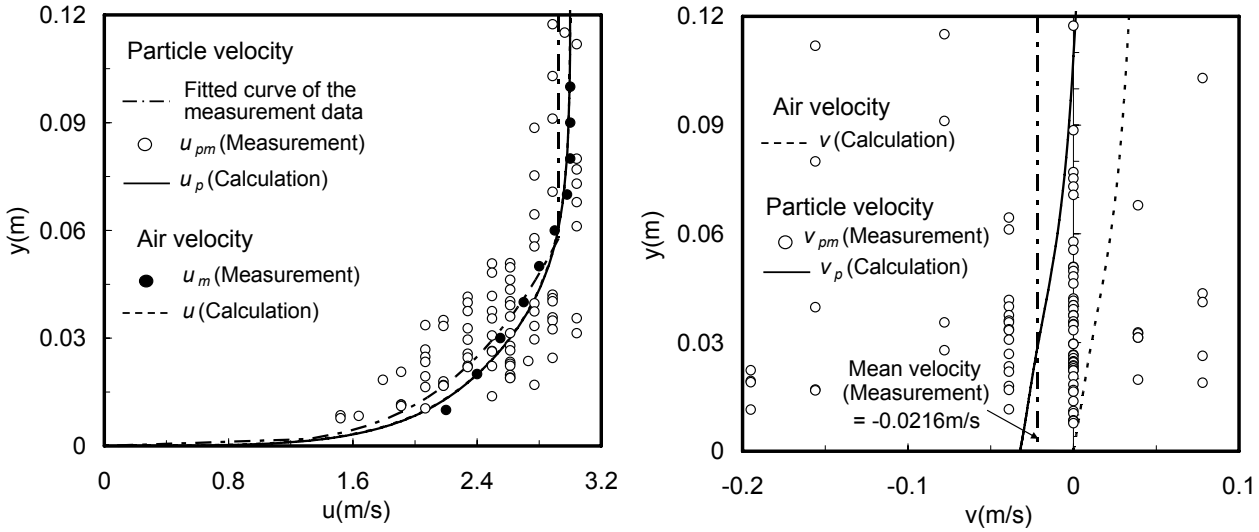

(a) *x*-direction **(b) *y*-direction**

Fig.5 Comparison of the measured and the calculated velocity profiles (*U*=3m/s)

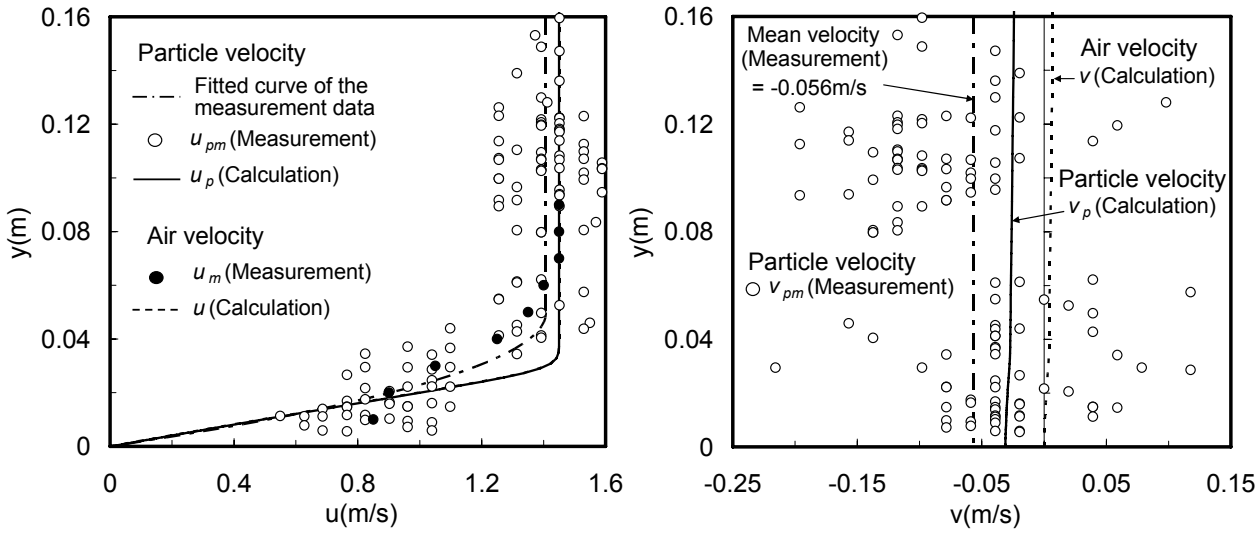

(a) *x*-direction **(b) *y*-direction**

Fig.6 Comparison of the measured and the calculated velocity profiles (*U*=1.5m/s)

In each figure, the measured particle velocities u_{pm} and v_{pm} (Both are empty circle) are scattered, because the resolution for measuring the path line length in the particle images is low. However, considering the mean value of the measurement, the calculated particle velocities u_p and v_p (Both are solid line) agree well with the mean value of u_{pm} and v_{pm} (Both are dot-and-dash line), respectively in each figure. Consequently, we can predict the particle behavior in wind by this calculation method.

In Fig.5(b) and 6(b), both the calculated velocity profiles v and v_p are the same shape, and one lies on top of the other by moving horizontally. This difference between v and v_p is approximately constant, and this constant difference of the velocities seems to equal the terminal velocity of the test particle V_t (ref. Table 1). In Fig.7, the calculated particle velocity v_p is compared with the velocity in which the terminal velocity V_t is pulled from the calculated air velocity v.

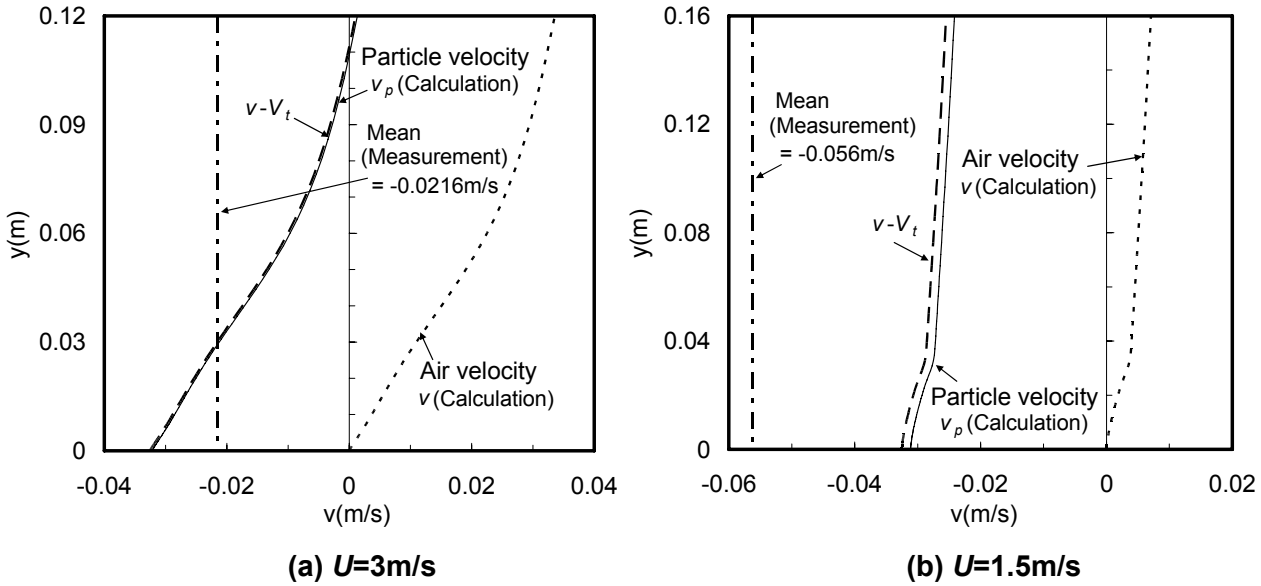

Fig.7 Comparison of v_p and v-V_t

Fig.7(a) shows that v_p and v -V_t are equal. Fig.7(b) shows that v_p and v -V_t are almost equal and the difference between v_p and v -V_t is approximately less than 5%. Consequently, we can predict the particle velocity by using air and its terminal velocity.

POLLEN INVASIVE BEHAVIOR

We numerically simulated the behavior of the pollen invading our nose holes to clear the influence of air velocity of suction breath on the pollen invasion. Assuming two-dimensional steady flow, we calculated the air and the test particle flows around a front face in enough wide area. A schema of the calculation grid (coordinate system) is shown in Fig.8. As a human face, especially around the nose hole, has a complex geometry, we used Body Fitted Curvilinear coordinate system (BFC) that is shown in Fig.8. This coordinate system BFC is different from the preceding chapter (the preceding chapter: Cartesian coordinate), but the basic method of this calculation is the same as the preceding chapter and the governing equations of this calculation are as follows: (1) Continuity equation, (2) 2-D Navier-Stokes equations, (3) x and y Particle momentum equations.

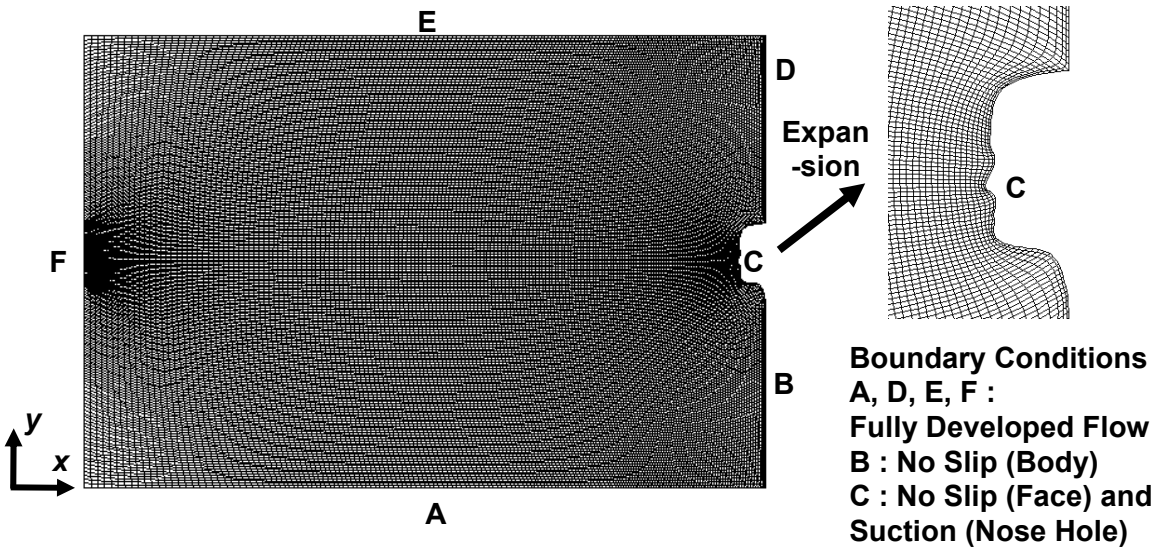

Fig.8 Schema of the calculation grid and the boundary conditions

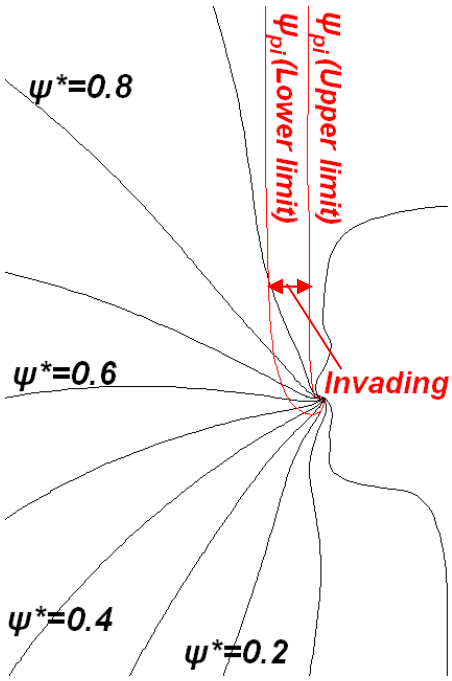

(a) Streamlines of the air and the particle flow
(ψ^* : Air , ψ_{pi} : Flow of the invasive particle)

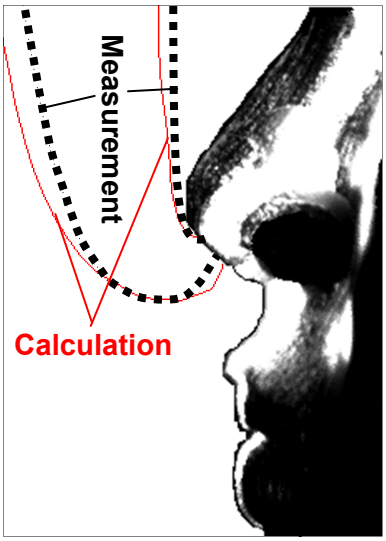

Comparison of the upper and the lower limit lines between the calculation and the measurement

(b) Streamlines of the flow of the invasive particle

Fig.9 Calculated streamlines (V_S =0.4m/s)

The outline of boundary conditions is also shown in Fig.8, but the following explanations are added.
(1) The air velocity of suction breath into the nose hole V_S is changed from 0.4m/s to 4.1m/s according to real human breath. (The suction air velocity into the nose hole is less than about 2m/s when a person takes in breath at rest. However, assuming the person to be active, we decided the range of V_S)
(2) Test particles are distributed in a uniform concentration.
(3) Test particles fall into the calculation field through the upper boundary E with the terminal velocity.

The calculation method of this study is only 2-D. However, we had reported how the 2-D calculation differed from an actual phenomenon and got the following results (2007).
(1) Near the nose hole, the agreement between 2-D calculations and measurements is good.
(2) The difference between 2-D calculation and measurement is large with the distance from the nose hole.

Furthermore, by 2-D calculation, we think it is possible to predict the relative difference of the invasive pollen amount in the air velocity of suction breath.

The calculated air and test particle streamlines are shown in Fig.9. In Fig.9, the streamlines of the particle flow are shown as "Upper limit" and "Lower limit". These limit lines mean the range of invasion. The suction airflow carries the test particles in-between these two limit lines into the nose hole. When paraphrasing, the test particles outside the two limit lines fall on the ground or body. Fig.9(a) also shows that the air streamlines are distributed radially and almost uniformly. In this case, the breath air is sucked from all direction because the air velocity of suction breath V_S is low.

Fig.9(b) shows the comparison of the limit streamlines near the nose hole between the calculation and the measurement. It is written in the above mentioned that the invasion range of the calculation is wider than the measurement because this calculation is 2D. However, this difference is a bit and this calculation almost agrees with the measurement.

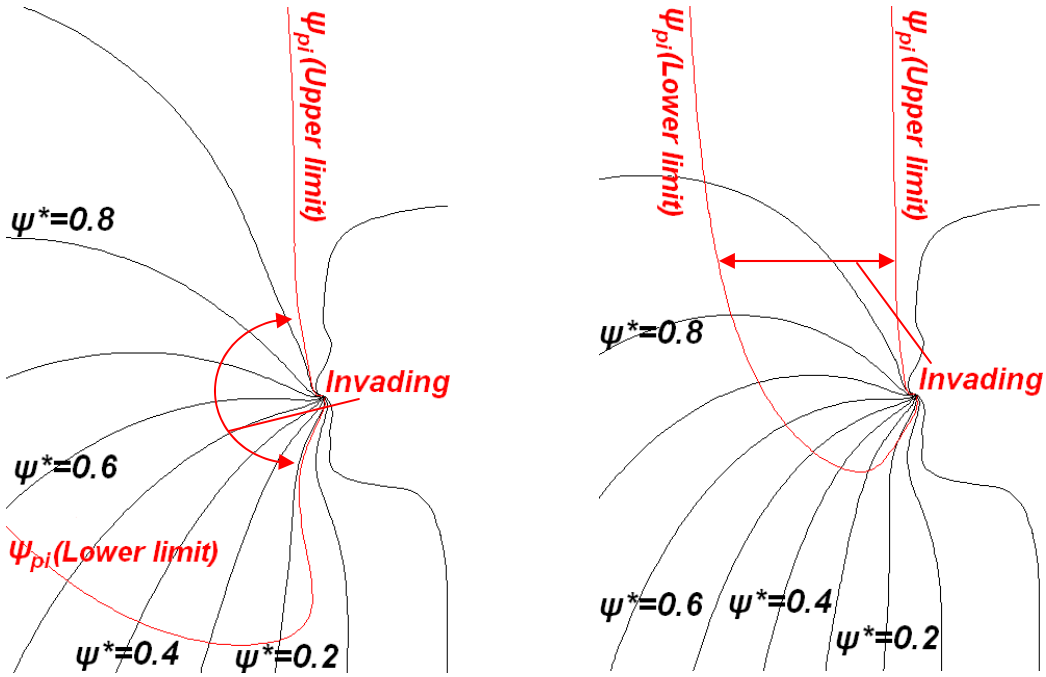

(a) V_S=4.1m/s **(b) V_S=1.55m/s**

Fig.10 Streamlines of the air and the particle flow
(ψ^* : Air , ψ_{pi} : Flow of the invasive particle)

The similar calculation results are shown as Fig.10. Fig.10(a) and (b) are the results of V_S =4.1m/s and V_S =1.55m/s, respectively. Fig.10 shows the invasion range in-between two limit lines is wider with the faster suction velocity V_S =4.1m/s and the breath air is mainly sucked from the lower part under the nose hole.

In Fig.9 and 10, we can notice that all suction air into nose hole doesn't include the test particles and the air without the particles is also sucked. The amount of the invasive particles may be varied according to the air velocity of suction breath. The relation between the suction velocity into the nose hole V_S and the invasion rate is shown as Fig.11. Invasion rate means the mass flow rate ratio of the suction air with particles to the entire suction air.

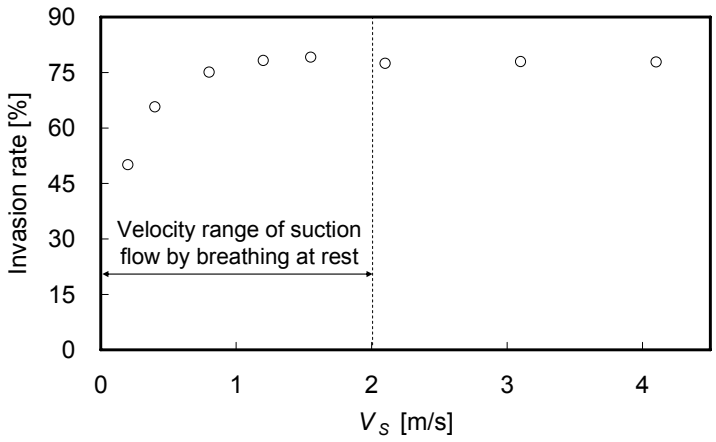

Fig.11 Relation between the air velocity of suction breath V_S and the invasion rate

Fig.11 shows that the invasion rate increases as V_S is fast, but it is nearly constant in more than V_S =1.0m/s. When a person stops his breath V_S=0.0m/s, invasion rate must be zero. Consequently, we think that Fig.11 shows the valid result.

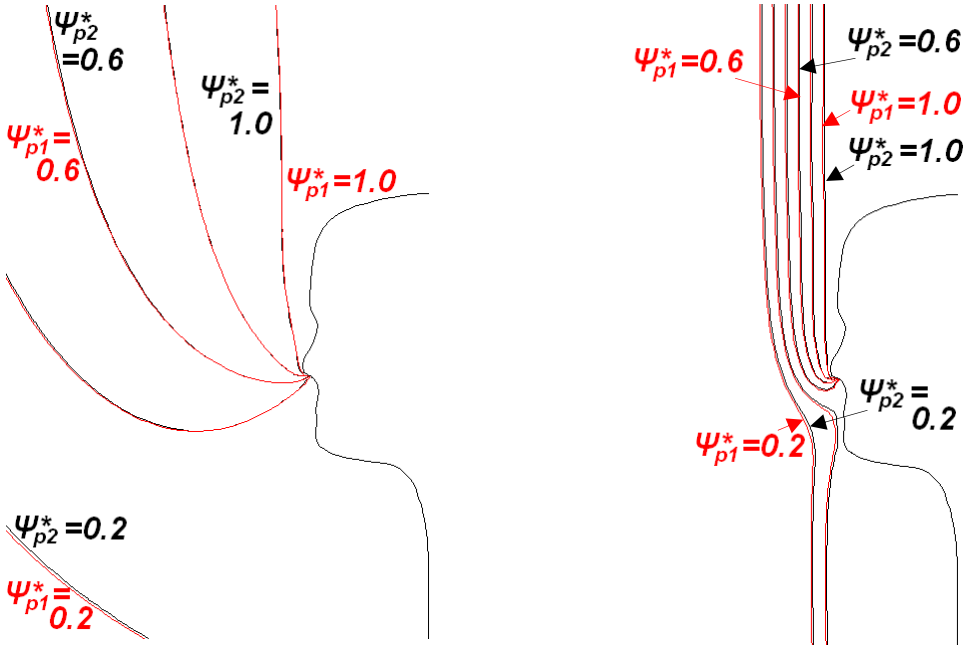

(a) V_S =4.1m/s **(b) V_S =1.55m/s**

Fig.12 Comparison of two kinds of streamlines of the particle flow ψ^*_{p1} and ψ^*_{p2} ψ^*_{p1} is calculated by u_p and v_p. ψ^*_{p2} is calculated by u and v -V_t.

Fig.5(a) and Fig.6(a) show that u_p equal u and Fig.7 shows that v_p and $v - V_t$ are approximately equal. We calculated the streamlines of the particle flow by using u and $v - V_t$ instead of u_p and v_p. Fig.12 shows these results. These two kinds of streamlines ψ^*_{p1} and ψ^*_{p2} are calculated by using (u_p, v_p) and (u, $v - V_t$) respectively. These are almost equal. We can predict the scattering behavior like this study by using air and particle terminal velocity.

CONCLUSION

The results obtained by this study are as follows.

(1) The terminal velocity V_t of the Japanese cedar pollen is measured, and the mean terminal velocity V_{tm} and the aerodynamic diameter d_a are decided as V_{tm}=38mm/s and d_a=35μm respectively.

(2) The pollen scattering behavior can be predicted by considering only the drag force (Stokes' Law for drag) in the momentum equations. In addition, the pollen (particle) horizontal and vertical velocities nearly equal the horizontal wind velocity u and the vertical wind velocity v minus terminal velocity V_t respectively.

(3) The air velocity of suction breath influences the rate of the pollen invasion into the nose hole. This rate decreases with the low suction velocity but is nearly constant in more than the suction velocity V_S =1.0m/s.

REFERENCES

Tang, H., Fujita, T., Seta, A., Fukui, M., Yamada, M., Suematsu, K., Hashiguchi, K., and Ookubo, K., (2007), "The measurement of the particle diameter and density of Japanese cedar pollen, and its terminal velocity and the measurement method of its concentration (in Japanese)", The proceedings of The 19th Spring Meeting of Japanese Society of Allergology, 373.

Ohashi, E., and Ooka, R., (2001), "Indoor Air-Pollution by Japanese Cedar Pollen (2) – Measurement of Particle Diameter and Weight of Cedar Pollen, and its Aerodynamic Diameter – (in Japanese)", The proceedings of The Annual Meeting of Architectural Institute of Japan (Kantou), 939-940.

Nakane, I., and Ide, T., (2007), "Prediction of the suspending and scattering pollen flow behavior (in Japanese)", Journal of Japan Society for Simulation Technology, **26**(2), 37–40.